nature physics

LETTERS

https://doi.org/10.1038/s41567-020-0809-9

Chromatic neuronal jamming in a primitive brain

Margarita Khariton[1,4], Xian Kong[2,4], Jian Qin[2]✉ and Bo Wang[1,3]✉

Jamming models developed in inanimate matter have been widely used to describe cell packing in tissues[1–7], but predominantly neglect cell diversity, despite its prevalence in biology. Most tissues, animal brains in particular, comprise a mix of many cell types, with mounting evidence suggesting that neurons can recognize their respective types as they organize in space[8–11]. How cell diversity revises the current jamming paradigm is unknown. Here, in the brain of the flatworm planarian *Schmidtea mediterranea*, which exhibits remarkable tissue plasticity within a simple, quantifiable nervous system[12–16], we identify a distinct packing state, 'chromatic' jamming. Combining experiments with computational modelling, we show that neurons of distinct types form independent percolating networks barring any physical contact. This jammed state emerges as cell packing configurations become constrained by cell type-specific interactions and therefore may extend to describe cell packing in similarly complex tissues composed of multiple cell types.

Jamming behaviours have been extensively studied in inanimate systems undergoing liquid-to-solid transitions, including foams, gels and emulsions[17–21]; more recently, similar concepts have been explored to describe cellular packing in biological tissues[1–7]. In physical systems, jamming transitions are controlled by a set of canonical variables: density, temperature and stress[18,20,21]. In tissues, these variables have been linked to cellular properties, including shape, migration and mechanics[4,6]. However, cell diversity has not been accounted for in the current framework of jamming, despite complex tissues being composed of many distinct cell types. In particular, neural tissues possess extremely high cell diversity and it is well known that neurons can recognize and interact with their respective types as they organize in space[8,9,22]. A neuron can avoid other neurons of its same type even when they are several cell body sizes apart, mediated by a variety of broadly conserved biological mechanisms (Fig. 1a and Supplementary Note 1)[10,11,22]. This repulsion causes homotypic neurons to organize into two-dimensional (2D) arrays with regular interneuronal spacing in sensory systems[10,11,22,23]. How these type-specific interactions organize cells in more complex three-dimensional (3D) tissues remains unknown.

To address this question, we propose a new jamming transition, which is controlled by the cell diversity of a tissue and thereby represents a dimension orthogonal to previously characterized jamming behaviours. In previous studies, the jamming state manifests as the positions and shapes of cells are constrained by their physical neighbours to give rise to a solid-like mechanical state[3–7]. Here, cell type adds an additional degree of freedom independent of tissue mechanical state, which can be progressively reduced as the cell diversity of a tissue decreases (Fig. 1a). At a critical number of cell types, homotypic repulsion becomes so abundant throughout the tissue that it limits the possible packing configurations of cells. Inspired by the colour map problem[24], we term this transition chromatic jamming.

We demonstrate chromatic jamming through both experimental and computational model systems. Experimentally, we use quantitative 3D imaging to investigate neuronal packing within the brain of the planarian *Schmidtea mediterranea* (Fig. 1b), one of the most basal organisms known to have a demarcated central nervous system, which contains several dozen neuronal types in a bilobed structure of densely packed neurons[13,25–28] (Fig. 1c,d and Supplementary Figs. 1 and 2). Importantly, the total number of neurons in the planarian brain scales linearly with animal size and can vary by more than an order of magnitude, from thousands to tens of thousands, while the number density of each neuronal type remains nearly constant[14].

With the high genetic similarity to the vertebrate nervous system[13,15,25,28], the planarian brain also provides the simplicity necessary for precisely determining individual neuronal positions. We acquired 3D confocal images of non-overlapping neuronal types using RNA fluorescence in situ hybridization (RNA-FISH) against a panel of neuropeptide genes, each specifically labelling the cell bodies of a distinct type of peptidergic neuron[13,14,28,29] (Fig. 1d and Supplementary Figs. 1 and 2). Our imaging resolution of 350 nm lateral, 700 nm axial, is sufficient to resolve single cells with an average diameter of ~6 μm using automated imaging analysis.

Two essential features are evident regarding the type-specific packing organization. First, despite the dense packing of neurons throughout the brain space, homotypic neurons are rarely in direct physical contact, consistent with the property of homotypic repulsion[9]; they do not organize into regular mosaic patterns either, unlike the well studied 2D sensory systems[9,11,23]. Second, in alignment with previous reports in other animals (for example, fruit fly and mouse)[9,10,22], no long-range interaction is observed between heterotypic neurons (Supplementary Fig. 3), allowing us to treat individual neuronal types separately.

To quantify the packing structure within each neuronal type, we located the centroids of individual neuronal cell bodies and identified their nearest homotypic neighbours using Voronoi tessellation, which has been used extensively to define neuronal tiling patterns[30–32] (Fig. 1e). Figure 1f plots the centroids coloured according to the number of their homotypic nearest neighbours, n, with more examples shown in Supplementary Fig. 2. Although large variations in n between individual cells are observed, no long-range spatial heterogeneity is apparent. Figure 2a shows that the average number of nearest neighbours, $\langle n \rangle = 14 \pm 0.2$, is stable over various neuronal types and across a wide range of brain sizes. This value is in good agreement with that of classic 3D random close packings in particulate matter[17–20].

If neurons do in fact pack into a jammed state with respect to their homotypic neighbours, then only a fraction of nearest

[1]Department of Bioengineering, Stanford University, Stanford, CA, USA. [2]Department of Chemical Engineering, Stanford University, Stanford, CA, USA. [3]Department of Developmental Biology, Stanford University School of Medicine, Stanford, CA, USA. [4]These authors contributed equally: Margarita Khariton, Xian Kong. ✉e-mail: jianq@stanford.edu; wangbo@stanford.edu

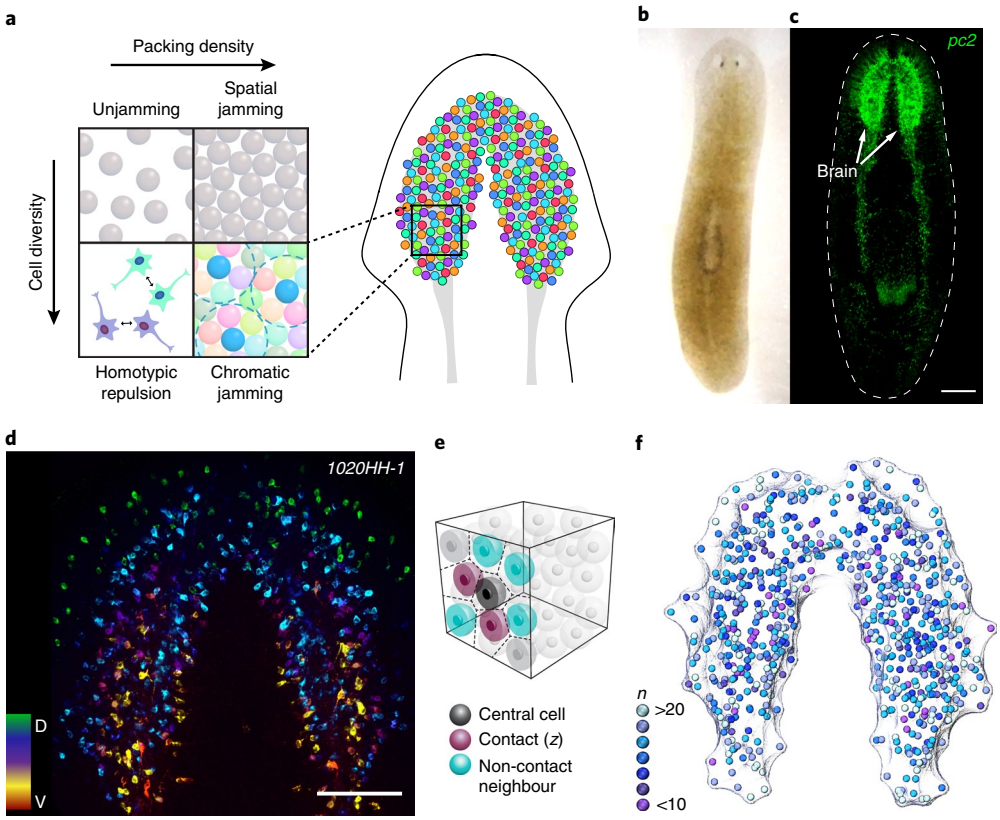

Fig. 1 | The planarian brain allows quantification of neuronal packing with single-neuron resolution. a, Diagram illustrating particle packing of a system as a function of packing density and cell diversity: low density and diversity give rise to an unjammed system (top left), while increasing the packing density in homogeneous tissues results in the conventional spatially jammed state (top right). Homotypic repulsion (bottom left) gives rise to a chromatically jammed state (bottom right), as in the spatial organization in neural tissues composed of numerous distinct neuronal types. Dashed circles: range of cell type-specific interactions. **b**, Bright-field image showing the gross morphology of the planarian *S. mediterranea*. **c**, Fluorescence microscopy image (maximum intensity projections of confocal stack) depicting the planarian nervous system as stained for the neuronal marker *prohormone convertase 2* (*pc2*), which is expressed in all peptidergic neurons[27,29]. Scale bar: 200 µm. **d**, Depth-coloured projection image showing RNA-FISH of neuropeptide *1020HH-1* to reveal the spatial distribution of *1020HH-1*$^+$ peptidergic neurons in the planarian brain. Colour map: dorsal to ventral. Scale bar: 100 µm. **e**, Illustrative diagram of homotypic neighbours and contacts. For a given cell (black), the homotypic nearest neighbours (blue and purple) are defined by adjacent Voronoi tessellation units, and neighbours in geometric contact (purple) are defined as units with touching enclosing spheres. Solid spheres, cell body centroids; translucent zones, range of homotypic repulsion. **f**, Centroids of *1020HH-1*$^+$ peptidergic neurons determined from the image in **d**. Colours represent *n* of each individual neuron, measured by Voronoi tessellation.

homotypic neighbours should be in geometric contact[17,18]; rather than touching physically and bearing mechanical force, same-type cells instead experience 'contact' by falling within one another's exclusion volume of homotypic repulsion (Fig. 1e). This fraction of cells in contact must be larger than the characteristic value of random loose packing (the loosest way to pack particles), and its average should be independent of local variables such as packing unit size[17–19]. To test these predictions, we fit the largest possible sphere (that is, the exclusion volume) to each Voronoi unit and define geometric contacts as occurring between touching spheres, with packing unit size (d) as the diameter of the fit sphere. As homotypic repulsion is typically mediated by diffusive molecules or transient interactions between long neuronal processes that may extend in all possible directions[9–11], the nearly spherical exclusion volume (which does not necessitate spherical cells) is a reasonable first approximation. The average unit size, $\langle d \rangle$, is approximately 18 µm, corresponding to three cell sizes, consistent with the expectation that neurons prohibit direct contact of homotypic neighbours[9–11,22,23]. The average fraction of contact neighbours, $\langle z/n \rangle$, ranges from 0.4 to 0.6 (Fig. 2b), which is above the reported values of random loose packing (0.3–0.4) yet is consistent with random close packing near the jamming transition in non-living particulate systems[17–19]. As predicted, $\langle z/n \rangle$ is also largely independent of neuronal type and Voronoi unit size.

The fluctuations of these geometric measures also exhibit hallmarks of the jammed state. We chose the granocentric jamming model[17,19] for quantitative comparison, as it provides closed-form expressions for the distributions of nearest neighbours and contacts, which serve as signatures of jammed configurations in close-packed systems. These measures are particularly useful when directly measuring dynamics is infeasible, as in our experimental system, where the neurons must be held in space to maintain their connections so that they may support vital physiology. We measured the distributions $P(n)$, $P(z)$ and $P(d)$ for three representative neuronal populations and found each of the distributions to agree with the predictions of the granocentric model, with no free fitting parameter (Fig. 2c). The wide distributions are consistent with heterogeneous brain structures, which contain other cell types and extracellular components, causing cell-specific homotypic repulsion to extend over a broad range of length scales (Supplementary Fig. 1).

The geometric signatures collectively establish the impacts of type-specific interactions on the packing state of neurons. To test if homotypic contacts alone are sufficient to build up to a chromatic

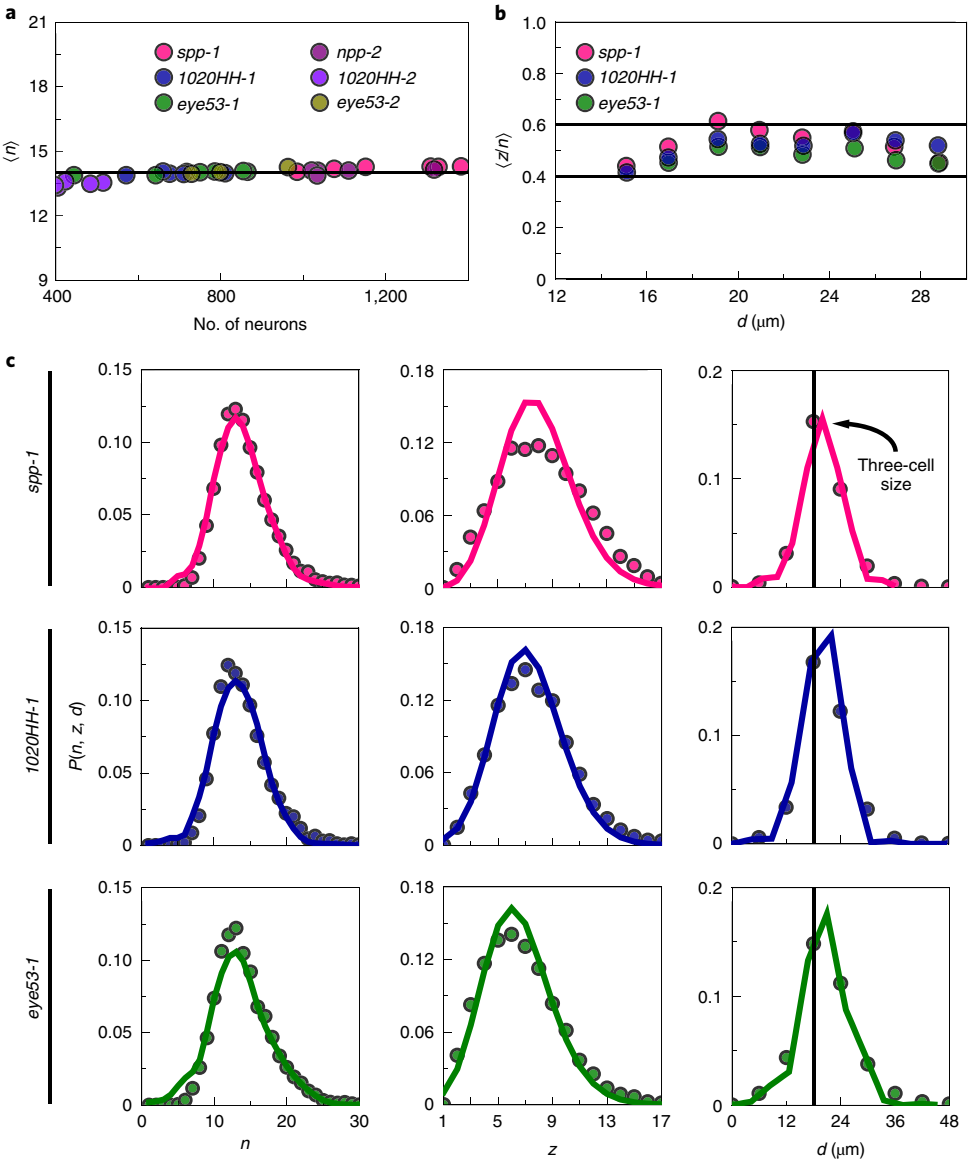

Fig. 2 | Neuronal packing exhibits geometric hallmarks of jamming. a, The average number of nearest neighbours, $\langle n \rangle$, plotted against total number of neurons in respective populations, is invariant for all six measured peptidergic neuronal populations from 34 planarians of various sizes. Horizontal line: $\langle n \rangle = 14$. **b**, The average fraction of contact neighbours, $\langle z/n \rangle$, plotted against packing unit size (d), falls in the range of 0.4–0.6 (horizontal lines) regardless of packing unit size and neuronal type. **c**, Probability distributions of n, z and d for three representative peptidergic neuronal populations. Distributions of n and z are centred about 14 and 6.5, respectively, with the d distribution having a peak at 18 μm, equivalent to three cell sizes. Note that $P(n)$ spans the range from 5 to 25 and stands in contrast with the narrow distribution (12–17) expected from the packing of monodisperse units[17]. Symbols, experimental data; solid lines, granocentric model of jammed polydisperse soft particles[17,19].

jamming state, we constructed a minimum computational model that accounts for both physical and homotypic interactions. We modelled neurons as particles partitioned evenly into c types, with each type assigned a random representative colour (Fig. 3a). The range of repulsion between heterotypic particle pairs is one particle size, to account for volume exclusion, and that between homotypic pairs is three particle sizes, to match the experimentally measured average distances between homotypic neurons (Fig. 2c). Initial system configurations were generated randomly at a total packing density ϕ and equilibrated by shuffling particle positions to minimize total energy[33] (Supplementary Fig. 4a).

Several key deviations from conventional jamming are anticipated in our model. First, the extra constraints imposed by the long-range homotypic contacts should shift the jamming transition toward lower packing densities, the extent of which depends on the number of unique cell types. Furthermore, as the prevalence of homotypic contacts increases, the homotypic cells should 'cluster' in space—meaning that they fall within the three-cell-size range of homotypic repulsion of one another—and eventually propagate throughout the system to give rise to a 'percolation' transition[34]. Figure 3b illustrates these signatures: reducing c causes the homotypic cluster to grow until the largest homotypic contact cluster eventually spans the entire system, even if the overall ϕ remains below the conventional jamming transition point. Supplementary Fig. 5 shows that only under these percolating conditions does the abundance of homotypic contacts reach values consistent with experiments.

To identify the conditions that lead to the shifted jamming transition and emergent percolation transition, we constructed a phase

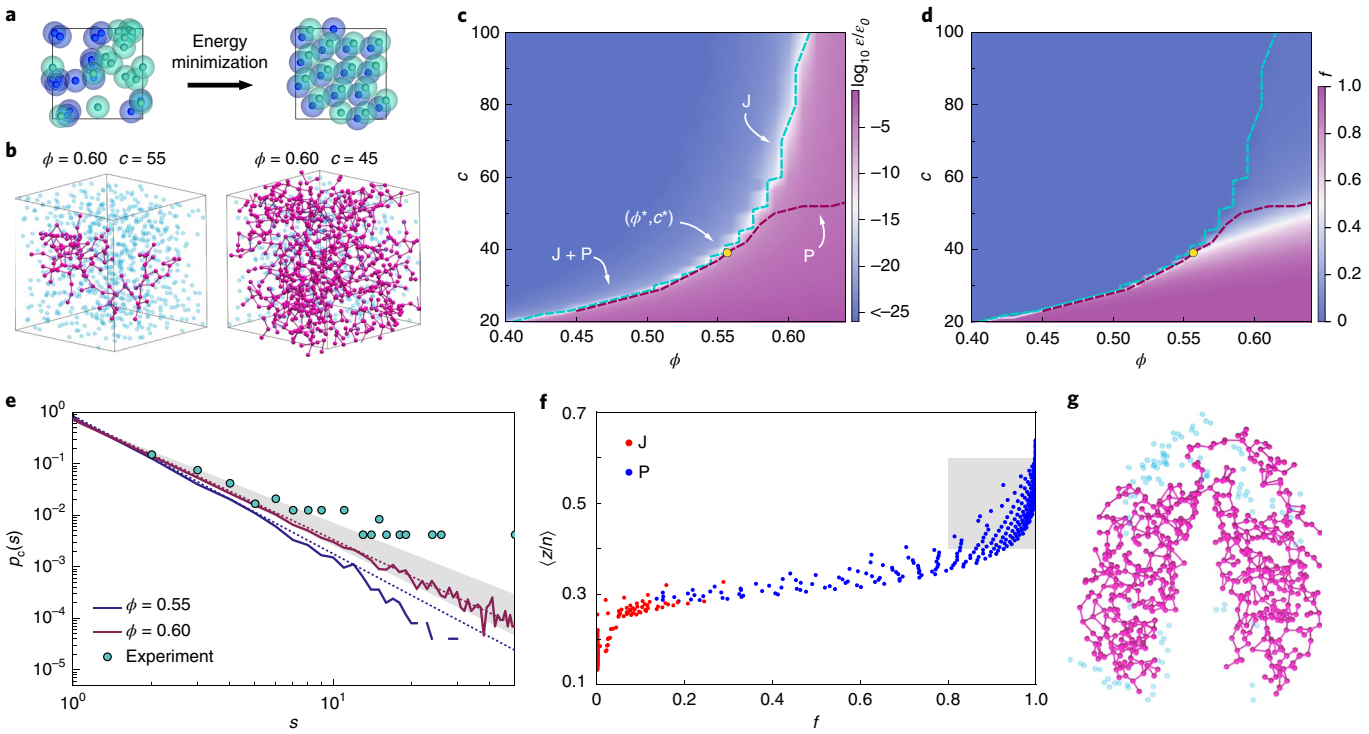

Fig. 3 | A chromatic jamming model for neuronal packing. a, Model schematic: blue and green particles represent distinct neuronal types, with a translucent zone around each representing the homotypic exclusion volume. **b**, Representative largest homotypic cluster (magenta) in chromatically unjammed (left) and jammed (right) states. Cyan: centroids of homotypic particles not in the largest cluster. **c**, Heat map showing residual energy per particle after equilibration as a function of c and ϕ. Cyan line, J jamming transition; red line, P percolation transition. The triple point, (ϕ^*, c^*), is localized at the intersection of J and P lines, below which jamming and percolation occur simultaneously (J + P). The range of c is set to match previous reports[13,25,26] that the planarian brain contains several dozen neuronal types. **d**, Heat map showing the fraction of particles belonging to the largest homotypic cluster (f) as a function of c and ϕ. **e**, Homotypic cluster size distributions near the percolation transition exhibit power-law scaling. Solid line, simulation; dashed line, power-law asymptotics; symbols, experimental distribution, obtained by lumping all neuronal types to gain statistics. Note that distributions below the triple point, where $\phi < \phi^*$, diverge from the power law at large cluster sizes (for example, $\phi = 0.55$). The grey zone specifies the regime with τ between 2 and 2.5. **f**, Model predictions of $\langle z/n \rangle$, plotted against f, for simulations that cross the J or P transition. The grey zone specifies the regime observed in experiments. **g**, Percolating homotypic cluster (magenta) detected in a *1020HH-1*$^+$ neuronal population of the planarian brain. Cyan: centroids of *1020HH-1*$^+$ neurons not in the percolating cluster.

diagram by systematically varying ϕ and c across a biologically realistic regime (Fig. 3c). At low ϕ, the system is at the unjammed state and the energy per particle (ε) is practically zero. At sufficiently high packing density, a finite minimum energy indicates a jamming transition (Supplementary Fig. 4b), at which all particle positions become constrained[20,21] through both physical and homotypic contacts (Supplementary Fig. 6). To verify the essential contribution of homotypic repulsion computationally, we measured the system rigidity past the jamming line and showed that it vanishes after turning off the homotypic interaction (Supplementary Fig. 7). The transition density ('J' line) increases with c and approaches the upper limit, the random close packing volume fraction in unicomponent systems[17–20], 0.64, when c becomes sufficiently large.

We then explored the percolation transition ('P' line) by measuring the fraction of particles belonging to the largest homotypic cluster, f, which serves as the order parameter in a percolating system[34]. Figure 3d shows that the regime in which f approaches unity in our model deviates from the jamming line, especially at high packing density. Quantitatively, the basic ansatz of percolation[34] states that the distribution $p(s)$ of homotypic clusters of size s near the transition has a universal power-law shape (Methods). We identified conditions under which the power-law distribution persists over the widest range of s, as $p(s)$ should deviate from the power law preceding and succeeding the transition (Fig. 3e and Supplementary Fig. 8). Intriguingly, the intersection of the jamming and percolation lines gives rise to a triple point (ϕ^*, c^*) = (0.56, 40) (Fig. 3c). Below ϕ^*, jamming and homotypic percolation occur simultaneously ('J + P' line), as the contribution of homotypic contacts dominates that of physical contacts (Supplementary Fig. 6b); above ϕ^*, percolation and jamming diverge.

An assumption of the present model is that each cell type comprises an evenly divided portion, yet in the true biological context the brain contains fractions of individual neuronal types that can vary considerably and is populated by numerous other cell types (for example, glial cells)[35–37] that may not be under the influence of homotypic interactions. To explore this assumption, we studied a model containing only two types of particle, one of which experiences homotypic repulsion and the other of which does not. We varied the total packing density and the relative fractions of the two particle types and found that the jamming and percolation lines overlap before the conventional jamming transition (Supplementary Fig. 9). This result suggests that the percolation of even a single cell type that has homotypic repulsion is enough to drive the system to cross the jamming transition.

The comparison of simulation and experimental results reveals that the planarian brain packs within the percolation regime—it supports the notion that cell type adds an independent configurational degree of freedom, since the homotypic percolation transition is distinct from the system mechanical rigidity transition. First, the size distribution of homotypic neuronal clusters at the percolation

transition should follow a power law[34], with the exponent $\tau \approx 2.2$, which is nearly constant along the P line (Supplementary Fig. 8). This is exactly as observed in the experiment, although finite-size effects—due to relatively small numbers of homotypic neurons in individual brains—limit the statistics of larger clusters and cause a deviation at the tail (Fig. 3e). Second, experimentally observed $\langle z/n \rangle \approx 0.4$–$0.6$ for homotypic neuronal neighbours should only exist after the percolation transition (Fig. 3f and Supplementary Fig. 5). This is distinct from the conventional jamming model, in which $\langle z/n \rangle$ is a function of packing density alone[17–19]. Third, large percolating homotypic clusters should be detectable in the percolation regime and are accordingly found in the planarian brain, as exemplified in Fig. 3g. The broad agreement between the experiment and the model is compelling. While the molecular mechanisms that drive neuronal tiling can vary (ranging from control of neighbouring neuronal differentiation to synaptic pruning or growth), and are expected to be influenced by non-neuronal cells and extracellular structures[9–11] (Supplementary Note 1), our model, despite its simplicity, suggests that homotypic interaction alone is sufficient to reproduce the observed statistical regularities in neuronal packing, regardless of the complex biological mechanism of control.

The chromatic jamming transition described here extends the classic notion of jamming regarding system rigidity[1,3,4,6,17,18,20] by introducing cell diversity as an orthogonal dimension. Cell type-specific interactions impose additional geometric constraints that favour a subset of packing configurations. Although hallmarks of such a state have been quantitatively verified in a basal nervous system, chromatic jamming may also provide a general physical framework for neurons to organize in other densely packed neural tissues. The structural constraints in chromatic jamming can have important physiological implications in a variety of biological processes, including neuronal differentiation, cell type diversification, and optimization of neuronal network connection efficiency. In addition, how cell type-specific interactions are influenced by cell shape, mechanics and motility, and inversely how cell type interactions change the mechanical and packing states of tissues in non-neural systems, are important avenues to explore. More broadly, this work reveals a living example of a complex network structure with multiple percolated subnetworks intercalating in space, which may find other applications, as in signal communication and graph optimization.

Online content

Any methods, additional references, Nature Research reporting summaries, source data, extended data, supplementary information, acknowledgements, peer review information; details of author contributions and competing interests; and statements of data and code availability are available at https://doi.org/10.1038/s41567-020-0809-9.

Received: 4 December 2018; Accepted: 21 January 2020;
Published online: 9 March 2020

References

1. Farhadifar, R., Röper, J. C., Aigouy, B., Eaton, S. & Jülicher, F. The influence of cell mechanics, cell-cell interactions, and proliferation on epithelial packing. *Curr. Biol.* **17**, 2095–2104 (2007).
2. Oswald, L., Grosser, S., Smith, D. M. & Käs, J. A. Jamming transitions in cancer. *J. Phys. D* **50**, 483001 (2017).
3. Atia, L. et al. Geometric constraints during epithelial jamming. *Nat. Phys.* **14**, 613–620 (2018).
4. Bi, D., Lopez, J. H., Schwarz, J. M. & Manning, M. L. A density-independent rigidity transition in biological tissues. *Nat. Phys.* **11**, 1074–1079 (2015).
5. Park, J. A. et al. Unjamming and cell shape in the asthmatic airway epithelium. *Nat. Mater.* **14**, 1040–1048 (2015).
6. Mongera, A. et al. A fluid-to-solid jamming transition underlies vertebrate body axis elongation. *Nature* **561**, 401–405 (2018).
7. Schötz, E. M., Lanio, M., Talbot, J. A. & Manning, M. L. Glassy dynamics in three-dimensional embryonic tissues. *J. R. Soc. Interface* **10**, 20130726 (2013).
8. Chklovskii, D. B., Schikorski, T. & Stevens, C. F. Wiring optimization in cortical circuits. *Neuron* **34**, 341–347 (2002).
9. Rockhill, R. L., Euler, T. & Masland, R. H. Spatial order within but not between types of retinal neurons. *Proc. Natl Acad. Sci. USA* **97**, 2303–2307 (2000).
10. Grueber, W. B. & Sagasti, A. Self-avoidance and tiling: mechanisms of dendrite and axon spacing. *CSH Perspect. Biol.* **2**, a001750 (2010).
11. Fuerst, P. G., Koizumi, A., Masland, R. H. & Burgess, R. W. Neurite arborization and mosaic spacing in the mouse retina require DSCAM. *Nature* **451**, 470–474 (2008).
12. Newmark, P. A. & Alvarado, A. S. Not your father's planarian: a classic model enters the era of functional genomics. *Nat. Rev. Genet.* **3**, 210–219 (2002).
13. Cebrià, F. et al. Dissecting planarian central nervous system regeneration by the expression of neural-specific genes. *Dev. Growth Differ.* **44**, 135–146 (2002).
14. Takeda, H., Nishimura, K. & Agata, K. Planarians maintain a constant ratio of different cell types during changes in body size by using the stem cell system. *Zool. Sci.* **26**, 805–813 (2009).
15. Mineta, K. et al. Origin and evolutionary process of the CNS elucidated by comparative genomics analysis of planarian ESTs. *Proc. Natl Acad. Sci. USA* **100**, 7666–7671 (2003).
16. Rink, J. C. Stem cell systems and regeneration in planaria. *Dev. Genes Evol.* **223**, 67–84 (2013).
17. Clusel, M., Corwin, E. I., Siemens, A. O. N. & Brujić, J. A 'granocentric' model for random packing of jammed emulsions. *Nature* **460**, 611–615 (2009).
18. Song, C., Wang, P. & Makse, H. A. A phase diagram for jammed matter. *Nature* **453**, 629–632 (2008).
19. Jorjadze, I., Pontani, L. L., Newhall, K. A. & Brujić, J. Attractive emulsion droplets probe the phase diagram of jammed granular matter. *Proc. Natl Acad. Sci. USA* **108**, 4286–4291 (2011).
20. O'Hern, C. S., Langer, S. A., Liu, A. J. & Nagel, S. R. Random packings of frictionless particles. *Phys. Rev. Lett.* **88**, 075507 (2002).
21. Liu, A. J. & Nagel, S. R. Jamming is not just cool any more. *Nature* **396**, 21–22 (1998).
22. Reese, B. E. & Keeley, P. W. Design principles and developmental mechanisms underlying retinal mosaics. *Biol. Rev.* **90**, 854–876 (2015).
23. Han, C. et al. Integrins regulate repulsion-mediated dendritic patterning of *Drosophila* sensory neurons by restricting dendrites in a 2D space. *Neuron* **73**, 64–78 (2012).
24. Wilson, R. *Four Colors Suffice: How the Map Problem Was Solved* (Princeton University Press, 2013).
25. Fraguas, S., Barberán, S., Ibarra, B., Stöger, L. & Cebrià, F. Regeneration of neuronal cell types in *Schmidtea mediterranea*: an immunohistochemical and expression study. *Int. J. Dev. Biol.* **56**, 143–153 (2012).
26. Fincher, C. T., Wurtzel, O., de Hoog, T., Kravarik, K. M. & Reddien, P. W. Cell type transcriptome atlas for the planarian *Schmidtea mediterranea*. *Science* **360**, eaaq1736 (2018).
27. Agata, K. et al. Structure of the planarian central nervous system (CNS) revealed by neuronal cell markers. *Zool. Sci.* **15**, 433–440 (1998).
28. Inoue, T. et al. Morphological and functional recovery of the planarian photosensing system during head regeneration. *Zool. Sci.* **21**, 275–283 (2004).
29. Collins, J. J. et al. Genome-wide analyses reveal a role for peptide hormones in planarian germline development. *PLoS Biol.* **8**, e1000509 (2010).
30. Duyckaerts, C. & Godefroy, G. Voronoi tessellation to study the numerical density and the spatial distribution of neurons. *J. Chem. Neuroanat.* **20**, 83–92 (2000).
31. Kay, J. N., Chu, M. W. & Sanes, J. R. MEGF10 and MEGF11 mediate homotypic interactions required for mosaic spacing of retinal neurons. *Nature* **483**, 465–469 (2012).
32. Wässle, H. & Riemann, H. J. The mosaic of nerve cells in the mammalian retina. *Proc. R. Soc. Lond. B* **200**, 441–461 (1978).
33. O'Hern, C. S., Silbert, L. E., Liu, A. J. & Nagel, S. R. Jamming at zero temperature and zero applied stress: the epitome of disorder. *Phys. Rev. E* **68**, 011306 (2003).
34. Stauffer, D. & Aharony, A. *Introduction to Percolation Theory* (Taylor and Francis, 1994). .
35. Morita, M. & Best, J. B. Electron microscopic studies of planaria: III. Some observations on the fine structure of planarian nervous tissue. *J. Exp. Zool.* **161**, 391–411 (1966).
36. Wang, I. E., Lapan, S. W., Scimone, M. L., Clandinin, T. R. & Reddien, P. W. Hedgehog signaling regulates gene expression in planarian glia. *eLife* **5**, e16996 (2016).
37. Roberts-Galbraith, R. H., Brubacher, J. L. & Newmark, P. A. A functional genomics screen in planarians reveals regulators of whole-brain regeneration. *eLife* **5**, e17002 (2016).

Methods

Animals. Asexual *S. mediterranea* (CIW4 strain) were maintained in the dark at 20 °C in ultrapure water supplemented with 0.5 g l^{-1} Instant Ocean Sea Salts and 0.1 g l^{-1} sodium bicarbonate. Planarians were fed calf liver paste once or twice weekly and starved for at least 5 d before all experiments.

Most imaging was performed on wild-type planarians, but to quantify the spatial arrangement of neurons in ectopic neural tissues (Supplementary Fig. 3) *β1-integrin* knockdown planarians were obtained with feeding of double-stranded RNA to induce RNA interference against the dd_Smed_v6_2017_0_1 transcript (PlanMine[38]), following the procedure described in refs. [39,40]. Double-stranded RNA was synthesized by in vitro transcription from the clone generated using oligonucleotide primers (5′ to 3′) GAACTCAA CACACAACGCCC and TCTCGACAGGGAACAATGGC to amplify the gene fragment from complementary DNA and clone into vector pJC53.2 (Addgene plasmid ID: 26536)[29]. Double-stranded RNA was mixed with liver paste at a concentration of 100 ng µl^{-1} and fed to planarians three times in 5 d. Planarians were head amputated 4 h after the final feeding and allowed to regenerate for 16 d before fixation.

RNA-FISH and image analysis. RNA probes against *pc2* and neuropeptide genes were synthesized as described previously, and FISH was performed following the established protocol[29,41]. To determine centroids of individual neurons using FISH signals, confocal stacks were obtained from a laser-scanning confocal microscope (Zeiss) at oversampled resolutions, that is, 350 nm lateral and 700 nm axial using a ×20 numerical aperture = 0.8 objective, as recommended by Imaris (Bitplane). The stacks were then resampled to give isotropic voxels and subjected to Gaussian filtering and background subtraction. Centroids of labelled cell bodies were segmented channel by channel with Imaris using parameters empirically determined to minimize the need for manual curation. The average cell size was determined to be ~6 µm, which also sets the upper limit for the fitting error in determining centroids. The centroid positions in three dimensions were then extracted for downstream statistical analyses.

Voronoi tessellation has been used broadly throughout the literature to evaluate the spatial distribution of cellular patterning[30–32], including that of the central nervous system—most widely, the retina[32]. Voronoi diagrams have proven useful in revealing unique spatial statistics associated with specific cellular populations and between experimental and control conditions in neural disorders[30,31]. In our analysis, Voronoi tessellation was performed on centroids using Delaunay triangulation through built-in functions in MATLAB. Since the homotypic cells are not physically touching, they are geometrically in contact if they fall within one another's exclusion zone established by the range of homotypic repulsion, which is assumed to extend in all directions. To define nearest neighbours that are also in contact, we first identified the closest neighbouring centroid for a given cell, then counted each of the nearest neighbours that were the same distance away—within an error tolerance range, which is the centroid fitting uncertainty, 6 µm—as being in contact. The granocentric model was plotted using the model and parameters specified previously[17,19], with inverse Laplace transform computed numerically.

Simulation and statistical analysis. Cells are represented as soft particles of uniform size interacting with a Hookean potential of the form $u(r) = 0.5\epsilon(1 - r/\sigma)^2$ for $r \leq \sigma$, and 0 otherwise, where $u(r)$ is the pairwise potential between two particles separated by distance r, and σ is the range of interaction. Every particle is randomly assigned a colour. The interaction range and strength for pairs of heterotypic particles are $\sigma = \sigma_0$ and $\epsilon = \epsilon_0$, whereas those for homotypic, concolour particles are $\sigma = 3\sigma_0$ and $\epsilon = 3\epsilon_0$. Homotypic particle–particle interaction is not affected by that of heterotypic particle pairs (and vice versa), and thus homotypic particles only experience long-range repulsion, as they are always separated at a distance larger than the range of heterotypic interaction in final packing configurations.

Every system contains N particles divided evenly into c types. Multiple system sizes were explored and the results reported are obtained from those performed on the largest system containing $N = 40{,}000$ particles to minimize size dependence. N was adjusted manually in each simulation to ensure that the number of particles for each type is identical. The simulation box is cubic and its dimension is determined through $\phi = N\pi\sigma_0^3/(6L^3)$, which gives a box edge, L, greater than $30\sigma_0$ for all densities studied. Energy minimization was carried out in LAMMPS[42] until the energy change per particle between consecutive simulation steps plateaued or reached a tolerance of $10^{-20}\epsilon_0$ (Supplementary Fig. 4). Steep descent was used first to relax the system to a configuration near the local minimum, followed by a Hessian-free truncated Newton algorithm to further minimize system energy. The periodic boundary condition was imposed.

To examine the effects of heterogeneity among different cell types, we also constructed binary systems that contain only two types of particle (Supplementary Fig. 9). In these systems, only particles of type 1 interact with each other through homotypic interaction, and particles of type 2 do not. Each system contains N/c particles of type 1 and $N - N/c$ particles of type 2, where c is the inverse of the fraction of type 1 particles, mirroring the number of types for evenly divided systems. All simulation procedures were the same as they were for evenly divided systems.

Three independent configurations were simulated for each condition and ϵ was computed by averaging across all configurations. The J point was then identified by the steepest jump of the energy, typically across several orders of magnitude, as varying packing density or colour number (Supplementary Fig. 4). The percolation line was identified following the basic ansatz of percolation[34], which states that $p(s)$ near the transition has a universal shape, $p(s) = s^{-\tau}g(s|c - c_h|^{1/\sigma})$, in which g is a cutoff function that plateaus for small s and damps rapidly for large s. The term $|c - c_h|^{1/\sigma}$ is the reciprocal of the typical cluster size, which vanishes at c_h. Geometric analysis was performed using Voronoi tessellation, similarly to the experimental protocol. Cluster analysis was based on homotypic interactions alone, where two same-colour particles separated by a distance shorter than a threshold l_c were assigned to the same cluster. A value $l_c = 2.99995\sigma_0$ was used to account for the homotypic repulsion with a truncation error. The transition point c_h is then located at the curve exhibiting the power-law distribution over the widest range of s, as $p(s)$ should deviate from the power law preceding and succeeding the transition (Supplementary Fig. 8).

The bulk and shear moduli of the jammed systems were obtained by perturbing the simulation box affinely and infinitesimally ($<10^{-8}$). The perturbations include compression, decompression for bulk modulus and application of shear strain for shear modulus. After perturbation, the systems were energy minimized again to reach an energy minimum that adapts to the perturbation. The stresses before and after the perturbation were used for modulus calculations[33].

Reporting Summary. Further information on research design is available in the Nature Research Reporting Summary linked to this article.

Data availability

The datasets generated and analysed within this study can be downloaded from https://github.com/xianshine/cJamming or are available from the corresponding authors on request.

Code availability

Analysis and simulation codes are available for public access on GitHub (https://github.com/xianshine/cJamming).

References

38. Brandl, H. et al. PlanMine—a mineable resource of planarian biology and biodiversity. *Nucleic Acids Res.* **44**, D764–D773 (2016).
39. Bonar, N. A. & Petersen, C. P. Integrin suppresses neurogenesis and regulates brain tissue assembly in planarian regeneration. *Development* **144**, 784–794 (2017).
40. Seebeck, F. et al. Integrins are required for tissue organization and restriction of neurogenesis in regenerating planarians. *Development* **144**, 795–807 (2017).
41. King, R. S. & Newmark, P. A. *In situ* hybridization protocol for enhanced detection of gene expression in the planarian *Schmidtea mediterranea*. *BMC Dev. Biol.* **13**, 8 (2013).
42. Plimpton, S. Fast parallel algorithms for short-range molecular dynamics. *J. Comput. Phys.* **117**, 1–19 (1995).

Acknowledgements

We thank Kejia Chen and Ke Chen for help with data analysis, R.H. Roberts-Galbraith and J.J. Collins III for experimental assistance during the early phase of this study and S. Granick, I. Riedel-Kruse, D.M. Sussman and P.N. Newmark for discussions. Plasmids that contain the planarian neuropeptide genes were provided by J.J. Collins III. This work is supported by the Burroughs Wellcome Fund through the CASI programme to B.W.

Author contributions

J.Q. and B.W. designed the research, M.K. and B.W. performed the experiments, M.K., X.K. and B.W. analysed the data, X.K. performed the simulation, X.K. and J.Q. analysed the simulation results and all authors wrote the paper.

Competing interests

The authors declare no competing interests.

Additional information

Supplementary information is available for this paper at https://doi.org/10.1038/s41567-020-0809-9.

Correspondence and requests for materials should be addressed to J.Q. or B.W.

Peer review information *Nature Physics* thanks Corey O'Hern and the other, anonymous, reviewer(s) for their contribution to the peer review of this work.

Reprints and permissions information is available at www.nature.com/reprints.

nature research

Corresponding author(s): Bo Wang & Jian Qin

Last updated by author(s): 2018/12/13

Reporting Summary

Nature Research wishes to improve the reproducibility of the work that we publish. This form provides structure for consistency and transparency in reporting. For further information on Nature Research policies, see Authors & Referees and the Editorial Policy Checklist.

Statistics

For all statistical analyses, confirm that the following items are present in the figure legend, table legend, main text, or Methods section.

n/a	Confirmed	
☐	☒	The exact sample size (*n*) for each experimental group/condition, given as a discrete number and unit of measurement
☐	☒	A statement on whether measurements were taken from distinct samples or whether the same sample was measured repeatedly
☒	☐	The statistical test(s) used AND whether they are one- or two-sided *Only common tests should be described solely by name; describe more complex techniques in the Methods section.*
☒	☐	A description of all covariates tested
☒	☐	A description of any assumptions or corrections, such as tests of normality and adjustment for multiple comparisons
☐	☒	A full description of the statistical parameters including central tendency (e.g. means) or other basic estimates (e.g. regression coefficient) AND variation (e.g. standard deviation) or associated estimates of uncertainty (e.g. confidence intervals)
☒	☐	For null hypothesis testing, the test statistic (e.g. *F*, *t*, *r*) with confidence intervals, effect sizes, degrees of freedom and *P* value noted *Give P values as exact values whenever suitable.*
☒	☐	For Bayesian analysis, information on the choice of priors and Markov chain Monte Carlo settings
☒	☐	For hierarchical and complex designs, identification of the appropriate level for tests and full reporting of outcomes
☒	☐	Estimates of effect sizes (e.g. Cohen's *d*, Pearson's *r*), indicating how they were calculated

Our web collection on statistics for biologists contains articles on many of the points above.

Software and code

Policy information about availability of computer code

Data collection	Large-scale Atomic/Molecular Massively Parallel Simulator (LAMMPS, 16 Mar 2018 version) was used to generate simulated packing configurations.
Data analysis	Cluster analysis of simulated data was performed using the scikit-learn toolkit (version 0.19.1). 3D Confocal microscopy images were analyzed using Imaris (Bitplane, version 7.6.2) and visualized using ZEN software (Carl Zeiss, version 2.3, blue edition). MATLAB and Python codes used to analyze the data, in addition to the 42 experimental datasets, are available publicly on GitHub (https://github.com/xianshine/cJamming).

For manuscripts utilizing custom algorithms or software that are central to the research but not yet described in published literature, software must be made available to editors/reviewers. We strongly encourage code deposition in a community repository (e.g. GitHub). See the Nature Research guidelines for submitting code & software for further information.

Data

Policy information about availability of data

All manuscripts must include a data availability statement. This statement should provide the following information, where applicable:

- Accession codes, unique identifiers, or web links for publicly available datasets
- A list of figures that have associated raw data
- A description of any restrictions on data availability

The datasets generated and analyzed within this study are available publicly on GitHub (https://github.com/xianshine/cJamming) or from the corresponding authors upon request.

Field-specific reporting

Please select the one below that is the best fit for your research. If you are not sure, read the appropriate sections before making your selection.

☒ Life sciences ☐ Behavioural & social sciences ☐ Ecological, evolutionary & environmental sciences

For a reference copy of the document with all sections, see nature.com/documents/nr-reporting-summary-flat.pdf

Life sciences study design

All studies must disclose on these points even when the disclosure is negative.

Sample size	34 planarians were imaged and analyzed for quantification of neuronal packing in the brain (Fig 1-3, Supplementary Fig 1), in addition to 8 planarians analyzed for heterotypic neuronal pairs (Supplementary Fig 2). These numbers were sufficient for generating the probability distributions for model comparison.
Data exclusions	No data were excluded from this study.
Replication	Experimental data were collected in 3 separate sessions, each of which reproduced results successfully. All data was collected using the same microscopy settings and experimental conditions, then analyzed with the same software and code, with no issues and full reproducibility between each.
Randomization	Not applicable to our study. Data were collected by localizing cells in the brains of wild-type planarians, with no group comparison or randomization necessary.
Blinding	Not applicable to our study.

Reporting for specific materials, systems and methods

We require information from authors about some types of materials, experimental systems and methods used in many studies. Here, indicate whether each material, system or method listed is relevant to your study. If you are not sure if a list item applies to your research, read the appropriate section before selecting a response.

Materials & experimental systems

n/a	Involved in the study
☐	☒ Antibodies
☒	☐ Eukaryotic cell lines
☒	☐ Palaeontology
☐	☒ Animals and other organisms
☒	☐ Human research participants
☒	☐ Clinical data

Methods

n/a	Involved in the study
☒	☐ ChIP-seq
☒	☐ Flow cytometry
☒	☐ MRI-based neuroimaging

Antibodies

Antibodies used	Primary antibodies: mouse anti-SYNORF1 (3C11, Developmental Studies Hybridoma Bank (DSHB)), 1:75 sheep anti-digoxigenin-POD, Fab fragments (11207733910, Roche), 1:1000 anti-DNP-HRP (FP1129, Perkin-Elmer), 1:300 anti-DNP-HRP (ZC0330, Vector Labs), 1:5000 Secondary antibody: goat anti-mouse IgG+IgM, peroxidase conjugated (115-035-044, Jackson ImmunoResearch), 1:250
Validation	All primary antibodies were verified in separate independent studies or prior co-localization experiments.

Animals and other organisms

Policy information about studies involving animals; ARRIVE guidelines recommended for reporting animal research

Laboratory animals	Asexual Schmidtea mediterranea (CIW4 strain) flatworms were used as the model organism of this study.
Wild animals	No wild animals were used in this study.

Field-collected samples	No field-collected samples were used in this study.
Ethics oversight	No Stanford IACUC protocol review or approval is required for studies involving planarian flatworms.

Note that full information on the approval of the study protocol must also be provided in the manuscript.